Constructing an Un-biased Whole Body Atlas from Clinical Imaging Data by Fragment Bundling

Matthias Dorfer[1,⋆], René Donner[1], and Georg Langs[1,2]

[1] CIR Lab, Department of Radiology, Medical University of Vienna, Austria
[2] CSAIL, Massachusetts Institute of Technology, Cambridge, MA, USA
{matthias.dorfer,rene.donner,georg.langs}@meduniwien.ac.at

Abstract. Atlases have a tremendous impact on the study of anatomy and function, such as in neuroimaging, or cardiac analysis. They provide a means to compare corresponding measurements across populations, or model the variability in a population. Current approaches to construct atlases rely on examples that show the same anatomical structure (e.g., the brain). If we study large heterogeneous clinical populations to capture subtle characteristics of diseases, we cannot assume consistent image acquisition any more. Instead we have to build atlases from imaging data that show only parts of the overall anatomical structure. In this paper we propose a method for the automatic contruction of an un-biased whole body atlas from so-called *fragments*. Experimental results indicate that the fragment based atlas improves the representation accuracy of the atlas over an initial whole body template initialization.

Keywords: Anatomical atlas construction, Medical imaging fragments, Average shape and intensity model, Landmark transformation accuracy.

1 Introduction

Models that represent common characteristics of a specific anatomical structure, or *atlases* are at the center of medical imaging analysis in the context of quantitative morphometric population analysis, or as a reference frame to summarize functional data across large cohorts. In computational anatomy anatomical atlases have been constructed for single organs such as the brain [3], or for entire body regions such as the abdomen [6]. Anatomical atlases help to automatically distinguish between healthy and pathological subjects [4] or to segment or annotate anatomical structures contained in the imaging data [8]. Existing approaches commonly rely on the presence of the same anatomical structure of interest in all examples that form the training data for the atlas, and the target data the atlas is applied to. This is feasible for organ specific studies, such as in

⋆ This work has received funding from the Austrian Sciences Fund (P 22578-B19, PULMARCH), EU (FP7/2007-2013) under grant agreements 318068 (VISCERAL), 257528 (KHRESMOI).

K. Mori et al. (Eds.): MICCAI 2013, Part I, LNCS 8149, pp. 219–226, 2013.

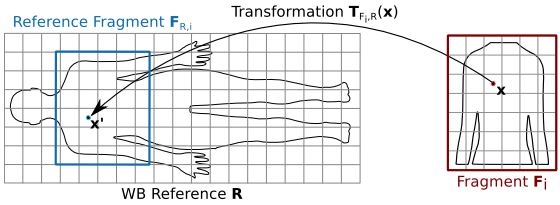

Fig. 1. Overview of fragment to WB reference space registration. The goal is to find a transformation $\mathbf{T}_{F_i,R}$ which registers a fragment $\mathbf{F}_i$ with the WB reference template $\mathbf{R}$.

neuroimaging, where the brain is the focus of analysis [1]. It is not feasible for building a representative model of the entire human body. In clinical practice, only those parts of the anatomy relevant for diagnosis are imaged [2]. We call these imaging data *fragments*. To use this data for population studies, to represent anatomical variability, or to identify characteristics of pathologies we need methodology to build an atlas from fragment data.

The contribution of this work is an atlas construction framework to construct an un-biased template from clinical medical imaging fragment data. Fragments acquired during clinical routine cover the human body in overlapping regions. The proposed atlas construction allows for the dense sampling of a wide range of anatomical regions in a clinical population. It goes beyond building and stitching individual atlases that represent individual anatomical regions. Furthermore, the atlas adds structure to arbitrary clinical imaging data examples, that constitute its training population. The framework provides functionality to localize the region of a fragment in relation to a Whole Body (WB) reference template and to register the fragment within the WB reference space. Based on the fragments the average shape and intensity template is updated. The method is closely related to Guimond et. al. [3] but extends it to image fragments. This fragment based model enables the bundling of imaging fragments within a single common WB reference space.

The results indicate that our approach is feasible, and is able to construct an atlas in situations where a large fraction of the data shows only part of the structure of interest. After an initial fit to a WB template the fragment registrations, and the template are updated and refined in an iterative process that further reduces bias.

2 Methods

Given a set of fragments $\mathbf{F}_1, ..., \mathbf{F}_N$, where $\mathbf{F}_i \in \mathbb{R}^{m_i \times n_i \times h_i}$, we seek to find a reference template $\mathbf{R} \in \mathbb{R}^{m \times n \times h}$ and corresponding transformations $\mathbf{T}_{F_i,R}$ so that $\mathbf{T}_{F_i,R}$ maps each position between the reference template and the individual fragment. To initialize the group-wise registration, all fragments are registered to a WB volume, that can either be a single individual, or the result of group-wise registration of multiple WB volumes. For each fragment the corresponding region (reference space fragment) $\mathbf{F}_{R,i}$ in $\mathbf{R}$ is determined. Then, the fragments $\mathbf{F}_i$ are

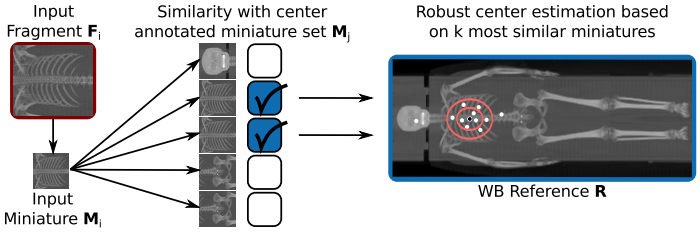

Fig. 2. Overview of miniature similarity based robust center estimation

registered to their corresponding region $\mathbf{F}_{R,i}$. After initialization the template is updated to represent both shape and appearance variation in the fragment population, and the fragments are registered to the updated template iteratively. This leads to an increasinlgy un-biased template $\mathbf{R}_F$ representing the population of fragments [3]. Fig. 1 illustrates all components contributing to the registration problem addressed. The main computation steps of the algorithm are: (1) For each fragment $\mathbf{F}_i$ estimate the center $\mathbf{c}_i$ in $\mathbf{R}$. (2) Estimate the corresponding reference fragment $\mathbf{F}_{R,i}$. (3) Non-rigidly register $\mathbf{F}_i$ to $\mathbf{F}_{R,i}$. (4) Compute updated fragment based shape and intensity population model $\mathbf{R}_F$ based on the registered fragments. In the following we describe the steps in detail.

2.1 Fragment Center Estimation

The first step to register $\mathbf{F}_i$ to $\mathbf{R}$ is to estimate its center position $\mathbf{c}_i$ in $\mathbf{R}$. This is based on calculating the appearance similarity of the fragment $\mathbf{F}_i$ and a set of fragments $\mathbf{F}_j^c$ with known center points $\mathbf{c}_j^c$, following an approach proposed in [2]. Fig. 2 provides an overview of the center estimation algorithm. For each $\mathbf{F}_j^c$ we construct a miniature $\mathbf{M}_j$ by resizing it to dimensions of $32 \times 32 \times 32$ voxels. $\mathbf{F}_i$ is downscaled analogously. We compute the Normalized Cross Correlation (NCC) and select those k miniatures for whom this similarity is highest.

Given the centers $\mathbf{c}_1^c, ..., \mathbf{c}_k^c$ of of the k top ranked miniatures, we calculate the median position, and keep the 50 percent of estimates closest to the median. The region containing these estimates is denoted as Region of Trimmed Estimates (RTE). From this set we calculate the center estimate by $\mathbf{c}_i = \frac{1}{k/2} \sum_{c_j^c \in RTE} \mathbf{c}_j^c$ for $\mathbf{F}_i$. This estimate is used to initialize the transformation and the fragment region in the WB template.

2.2 Fragment Region Estimation

Based on $\mathbf{c}_i$ we estimate the region in $\mathbf{R}$ corresponding to the fragment. We refine the fragment center estimate $\mathbf{c}_i$ as well as the region $\mathbf{I}_{F_{R,i}}$ (voxel coordinates) of the reference fragment $\mathbf{F}_{R,i}$ (intensity volume) with respect to $\mathbf{R}$ iteratively. The initial region $\mathbf{I}_{F_{R,i}}$ corresponding to the fragment is spanned by the bounding box, with same dimensions as the fragment, centered around $\mathbf{c}_i$, defined by coordinates of two opposite corners $\mathbf{x}_{cor1,i}$ and $\mathbf{x}_{cor2,i}$. The input fragment $\mathbf{F}_i$ is

affinely registered to the corresponding reference fragment $\mathbf{F}_{R,i} = \mathbf{R}(\mathbf{I}_{F_{R,i}})$ resulting in an affine transformation $\mathbf{T}^a_{F_i,R}$. Based on $\mathbf{T}^a_{F_i,R}$, we update $\mathbf{I}_{F_{R,i}}$. For the region update the two homogeneous corner coordinates $\mathbf{x}_{cor1,i}$ and $\mathbf{x}_{cor2,i}$ are transformed by the inverse of $\mathbf{T}^a_{F_i,R}$. i.e., $\mathbf{x}^1_{cor\,l,i} = \mathbf{T}^{a,-1}_{F_i,R}(\mathbf{x}_{cor\,l,i})$ with $l = 1, 2$. The updated corresponding region $\mathbf{I}^1_{F_{R,i}}$ of the fragment is now spanned by the transformed corner points $\mathbf{x}^1_{cor1,i}$ and $\mathbf{x}^1_{cor2,i}$ leading to an updated reference space fragment $\mathbf{F}^1_{R,i}$ and a rigid component $\mathbf{T}^r_{F_i,R}$ of the transformation $\mathbf{T}_{F_i,R}$. The updated center position $\mathbf{c}^1_i$ is computed as the arithmetic mean of the transformed corner points.

The localization procedure is iterated with the updated reference fragment until the region estimate $\mathbf{I}^k_{F_{R,i}}$ converges. We keep the affine transformation $\mathbf{T}^a_{F_i,R}$ of the final iteration k as initialization for the non-rigid registration.

2.3 Non-rigid Registration of the Fragment to the WB Template

The previous computation step estimates the corresponding reference space fragment $\mathbf{F}_{R,i}$ and region $\mathbf{I}_{F_{R,i}}$ of the input fragment $\mathbf{F}_i$ in the WB template $\mathbf{R}$. The final step of fragment to WB registration is the non-rigid registration of the query fragment $\mathbf{F}_i$ with the reference space fragment $\mathbf{F}_{R,i}$ yielding the non-rigid transformation $\mathbf{T}^{nr}_{F_i,R}$. For registration B-spline based Free Form Deformation (FFD) is used [7],[5]. The final result is an embedding of the non-rigidly registered fragment $\mathbf{F}'_i$ in the WB reference template $\mathbf{R}$ as well as the corresponding transformation $\mathbf{T}_{F_i,R} = \mathbf{T}^{nr}_{F_i,R} \circ \mathbf{T}^a_{F_i,R} \circ \mathbf{T}^r_{F_i,R}$.

2.4 Fragment Based Un-biased WB Reference Template Update

With the algorithm described in the previous subsections, we register fragments $\mathbf{F}_i$ with $i = 1, ..., N$ to a common reference template $\mathbf{R} \in \mathbb{R}^{m \times n \times h}$. In the first stage fragments are registered to an initial template $\mathbf{R}^0$. After the first iteration, this template is updated based on the fragment appearance, and deformation information, to obtain an un-biased template. For each fragment $\mathbf{F}_i$ we have the corresponding region $\mathbf{I}_{F_{R,i}}$ in $\mathbf{R}$, the reference fragment $\mathbf{F}_{R,i}$, the transformation $\mathbf{T}_{F_i,R}$, and the transformed fragment $\mathbf{F}'_i = \mathbf{F}_i(\mathbf{T}^{-1}_{F_i,R}(\mathbf{x}))$.

Based on these components the shape and intensity averaging, proposed by Guimond et. al. [3] is enhanced to a fragment based model. For a region constrained shape and intensity averaging we calculate for every voxel $\mathbf{x}$ in $\mathbf{R}$, the set of fragments $\mathcal{I}(\mathbf{x}) = \{i | \mathbf{T}^{-1}_{F_i,R}(\mathbf{x}) \in \mathbf{F}_i\}$ that contribute to it as well as the corresponding number of contributors $\mathbf{N}(\mathbf{x}) = |\mathcal{I}(\mathbf{x})|$. Based on $\mathbf{N}(\mathbf{x})$ the average fragment registration $\overline{\mathbf{F}}' \in \mathbb{R}^{m \times n \times h}$ is formalized as $\overline{\mathbf{F}}'(\mathbf{x}) = \frac{1}{\mathbf{N}(\mathbf{x})} \sum_{i \in \mathcal{I}(\mathbf{x})} \mathbf{F}_i(\mathbf{T}^{-1}_{F_i,R}(\mathbf{x}))$. The transformations of the fragments towards $\mathbf{R}$ are averaged in each voxel $\mathbf{x}$, i.e., $\overline{\mathbf{T}}_F = \mathcal{M}(\mathbf{T}^{nr}_{F_i,R})$ where $i \in \mathcal{I}(\mathbf{x})$. In practice we follow Guimond et. al [3] and estimate the mean by averaging the vector fields of the non-rigid transformations. We exclude rigid and affine transformations from un-biasing, since they mainly capture variability in image acquisition (e.g., body

Fig. 3. Construction results of the fragment based WB shape and intensity model $\mathbf{R}_F$ on 60 head, thorax, and abdomen fragments

region imaged, resolution), and assume that the population variability is encoded in the non-rigid component of the transformations. The fragment based average shape and intensity model $\mathbf{R}_F^1$ of iteration one is computed by applying the region dependent inverse average deformation $\overline{\mathbf{T}}_F^{-1}$ to the region dependent average intensity registration image $\overline{\mathbf{F}}'$. This results in $\mathbf{R}_F^1(\mathbf{x}) = \overline{\mathbf{F}}'(\overline{\mathbf{T}}_F^{-1}(\mathbf{x}))$ and draws the shape of the average intensity registration $\overline{\mathbf{F}}'$ towards the geometric population center of the training fragments [3]. The result is an un-biased fragment based model $\mathbf{R}_F^1$ representing the underlying fragment population $\mathbf{F}_1, ..., \mathbf{F}_N$. We proceed by again registering the fragments to this template, and updating the template $\mathbf{R}_F^k$ iteratively, until convergence.

3 Experimental Results

We evaluate the fragment based WBA construction on data that includes a single initial WB Computed Tomography (CT) volume $\mathbf{R}$ and 60 CT fragments $\mathbf{F}_i$ encompassing parts of the body including head, thorax, or abdomen. All volumes are isotropic and have a voxel dimension of 2 mm. In each fragment expert annotated bone landmarks are placed for evaluation, if present. They are used as reference for validation of registration accuracy, and the representational power of the atlas. The aim of the experiment is to show, (1) that the proposed method is capable to register medical imaging fragments containing locally limited anatomical regions to a common WB reference template $\mathbf{R}$ and (2) that the fragment based model $\mathbf{R}_F$ improves the representation of the imaging data in comparison to the initialization $\mathbf{R}$.

3.1 Experimental Setup

All 60 fragments $\mathbf{F}_i$ are registered with the WB template $\mathbf{R}$ resulting in the registered fragments $\mathbf{F}_i'$ and the corresponding transformations $\mathbf{T}_{F_i,R}$ (see sub

section 2.2 and Subsection 2.3). Fragment center estimation was based on 1200 annotated fragments. The registrations are used to compute the average fragment model $\mathbf{R}_F$ as described in sub section 2.4. Fig. 3 summarizes the results and shows the resulting fragment based model $\mathbf{R}_F$. Additionally the contribution of each training fragment $\mathbf{F}_i$ to the respective region of $\mathbf{R}_F$ is highlighted. In Fig. 3(c) blue rectangles indicate the bounding boxes of the fragments in the reference space.

After model computation all fragments are registered to the updated, unbiased fragment based template $\mathbf{R}_F$. The registration transformations $\mathbf{T}_{F_i,R}$ and $\mathbf{T}_{F_i,R_F}$ are applied to the coordinates of the landmarks annotated in the respective fragments. This yields landmark distributions containing the position estimates for each of the landmark positions in the two reference spaces $\mathbf{R}$ and $\mathbf{R}_F$. As evaluation measure the centroid of these landmark distributions as well as the mean distance of all landmarks in a distribution to their centroid are computed. If the method proposed is valid, the average distance to the centroids is expected to decrease for the fragment based model $\mathbf{R}_F$.

3.2 Evaluation of Landmark Transformation Accuracy

Fig. 4 shows the initial WB template $\mathbf{R}$ in comparison to the fragment based model $\mathbf{R}_F$. In addition to the maximum intensity projections the one, two, and three standard deviation areas of the transformed landmark distributions are visualized as ellipses. The numbers identify individual landmarks, annotated in the fragments. For both cases we registered the individual fragments to the template. We interpret a lower spread of the mapped positions as an indicator that the template is a better representative of the population. The fragment based model provides an improved representation of the fragment data, in particular in the abdominal region (landmark 32, 47-52). The bar plot in Fig. 5a presents the mean distances of the landmarks in a distribution to their centroid. The original WB template $\mathbf{R}$ is shown in blue; the fragment based model $\mathbf{R}_F$ in red.

In the abdominal region the transformation error decreases for the fragment based model in each of the seven landmarks (32, 47-52). The average distance over all seven landmarks decreases from 8.7 mm to 7.1 mm (-1.6 mm). Landmark 52 shows a maximum decrease of -2.58 mm. For the thorax region, the average distance shows a decrease for the first four landmarks (29, 30, 31, 33) and an increase for the remaining four of the eight landmarks (34, 47, 48, 49). The accuracy improvement over all thorax landmarks is summarized by an average transformation error decrease from 6.23 mm to 6.08 mm (-0.15 mm). The average distance to the center of the landmark distribution in the head fragments decreases for landmark 35, 36, 37, 41 and 42. The average distance of landmark 40 and 50 is not effected by the model. Landmark 38 and 39 show an increased distance. The accuracy improvement over all head landmarks is summarized by an average transformation error decrease from 3.96 mm to 3.82 mm (-0.14 mm).

Fig. 5b summarizes the average landmark transformation improvement achieved by the fragment based model for each landmark. Values below zero indicate that the model performs correct in the region of the respective landmark.

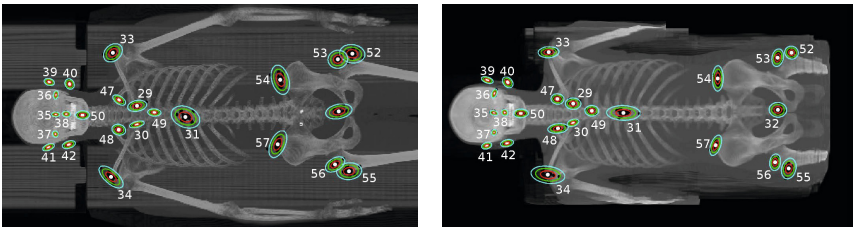

(a) Initial WB template $\mathbf{R}$. **(b)** Fragment based WB model $\mathbf{R}_F$.

Fig. 4. Landmark distributions before and after fragment based un-biased WB template computation. The ellipses indicate the distribution of landmarks mapped from all fragments the template. Ideally they should coincide. The fragment based model improves the agreement.

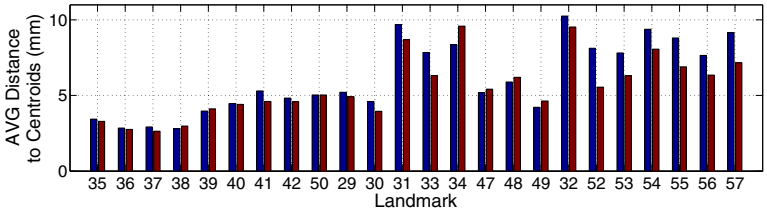

(a) Average distance of landmark distributions to their centroids.

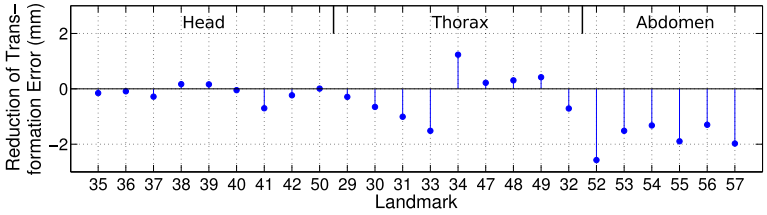

(b) Average improvement of landmark transformation accuracy.

Fig. 5. Landmark transformation accuracy of abdominal fragments before and after fragment based WB template update. (blue: initial WB reference $\mathbf{R}$, red: fragment based WB template $\mathbf{R}_F$).

The landmark transformation accuracy is increased for 16 landmarks, remains the same for landmark 40 and 50, and decreases for 6 of the 24 landmarks. The best results are achieved in the abdominal region.

This increased landmark transformation accuracy indicates that it is feasible to construct a whole body template from fragments. All fragment positions were located reliably during the initial center estimate. The decreased registration error of the landmarks shows that the fragment based WB model improves the representation of the underlying fragment population. Note that we did not explicitly evaluate the effect of pathologies present in the fragments at this point.

4 Conclusion

We propose methodology for constructing a WBA from fragments. The fragment based atlas is motivated by the fact, that typically individual medical imaging data recorded in hospitals do not cover the entire body region, while their inclusion into atlas building is necessary if we aim for a representative model of a large population [2,3]. This is relevant to represent the natural variability for model learning [3], disease characterization [4], or epidemiological research [9]. Existing approaches take only examples that cover identical anatomical structures into account (e.g., the brain [4]). The present work overcomes this limitation. The method estimates the position as well as the precise mapping between coordinates of a fragment and the WB reference fully automatically. In an iterative procedure the fragments are registered to a WB template, and this template is updated to reduce bias. The results show that our approach is feasible if the majority of the data consists of fragments, and reduces bias compared to an initial WB template.

References

1. Dale, A.M., Fischl, B., Sereno, M.I.: Cortical surface-based analysis – i. segmentation and surface reconstruction. Neuroimage 9, 179–194 (1999)
2. Donner, R., Haas, S., Burner, A., Holzer, M., Bischof, H., Langs, G.: Evaluation of fast 2d and 3d medical image retrieval approaches based on image miniatures. In: Müller, H., Greenspan, H., Syeda-Mahmood, T. (eds.) MCBR-CDS 2011. LNCS, vol. 7075, pp. 128–138. Springer, Heidelberg (2012)
3. Guimond, A., Meunier, J., Thirion, J.P.: Average brain models: A convergence study. Computer Vision and Image Understanding 77(2), 192–210 (2000)
4. Joshi, S., Davis, B., Jomier, B.M., Gerig, G.: Unbiased diffeomorphic atlas construction for computational anatomy. Neuroimage 23 (suppl. 1), 151–160 (2004)
5. Modat, M., Ridgway, G.R., Taylor, Z.A., Lehmann, M., Barnes, J., Hawkes, D.J., Fox, N.C., Ourselin, S.: Fast free-form deformation using graphics processing units. Comput. Methods Prog. Biomed. 98(3), 278–284 (2010)
6. Park, H., Bland, P.H., Meyer, C.R.: Construction of an abdominal probabilistic atlas and its application in segmentation. IEEE TMI 22(4), 483–492 (2003)
7. Rueckert, D., Sonoda, L.I., Hayes, C., Hill, D.L.G., Leach, M.O., Hawkes, D.J.: Nonrigid registration using free-form deformations: application to breast MR images. IEEE TMI 18(8), 712–721 (1999)
8. Sabuncu, M.R., Yeo, B.T.T., Van Leemput, K., Fischl, B., Golland, P.: A Generative Model for Image Segmentation Based on Label Fusion. IEEE TMI 29(10), 1714–1729 (2010)
9. Sabuncu, M.R., Balci, S.K., Shenton, M.E., Golland, P.: Image-driven population analysis through mixture modeling. IEEE TMI 28(9), 1473–1487 (2009)